ARMA 17-199

Clay-rich rocks as barriers for geologic CO_2 storage

Makhnenko, R.Y.

Department of Civil and Environmental Engineering, University of Illinois at Urbana-Champaign, Urbana, IL, USA

Vilarrasa, V.

Institute of Environmental Assessment and Water Research, Spanish National Research Council (IDAEA-CSIC), Barcelona, Spain

Associated Unit: Hydrogeology Group (UPC-CSIC), Barcelona, Spain

ABSTRACT: In geologic CO_2 storage, it is important to find a proper barrier material that will avoid or limit acidic fluid migration. Shales that are ductile and have high capillary entry pressure and low permeability can be considered as good candidates for the caprock. Faults may contain high percentage of clay and act as barriers for fluid flow in reservoirs. Experimental techniques have been developed to characterize the behavior of clay-rich materials at elevated pressures. Intact and remolded specimens of Opalinus clay – a Jurassic shale from Switzerland – are brought to the conditions of deep (> 1 km depth) geologic storage and fully saturated with in-situ brine. Poromechanical parameters and failure characteristics are measured in drained and undrained conventional triaxial compression experiments. CO_2 breaktrough pressure and permeability of shale are assessed in oedometric tests on thin (12 mm) samples. Experimentally measured parameters are used in numerical simulations to assess fault stability and the shaly caprock integrity for the case of geologic carbon storage, where cooling is likely to occur around injection wells. It is found that clay-rich faults may induce microseismic events, but without leading to CO_2 leakage.

1. INTRODUCTION

Safe long-term carbon dioxide (CO_2) geologic storage largely depends on caprock integrity (IEAGHG, 2011). The caprock may be especially altered at the early stages of injection, when the maximum overpressure is reached (Vilarrasa et al., 2010). As CO_2 is injected in the storage formation, it tends to advance through the top of it and below the caprock due to buoyancy (Hesse et al., 2008). Furthermore, the injected CO_2 will reach the bottom of the well at a colder temperature than that of the storage formation (Paterson et al., 2008). As a result, a cold region is formed around the injection well, but the cooling front advances much behind than the CO_2 plume interface (Vilarrasa and Rutqvist, 2017). Thus, the lower boundary of the caprock is in contact with CO_2 saturated pore water or pore fluid that consists almost of pure CO_2, which may be cold (Figure 1). These thermal and chemical interactions between the pore fluid and the caprock may change its material properties and affect stability.

Geomechanical stability is crucial to maintain the caprock sealing capacity because failure could increase permeability and potentially induce microseismicity (Verdon et al., 2011). Considering ductile clay-rich geomaterials (e.g., shales) as potential caprock has several advantages, including their thermal, chemical, and inelastic deformation characteristics. These characteristics minimize the effect of CO_2 injection on the sealing integrity and prevent the upward movement of CO_2 through the caprock's pore system due to the high entry pressure (Song and Zhang, 2013; Bourg, 2015).

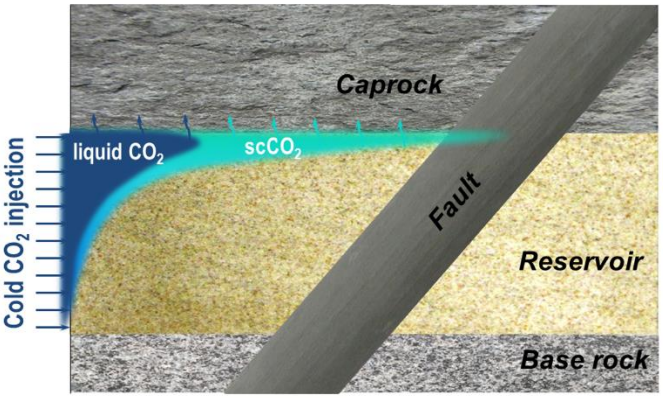

Fig. 1. Schematic representation of geologic carbon storage in a deep saline aquifer with a fault. A cold region is formed around the injection well and cools down the caprock. The caprock is also affected by geochemical reactions due to the acidic nature of CO_2 when it dissolves in water.

Another source of concern are faults (Rutqvist et al., 2016). Fault architecture is complex and may behave either as a barrier or a conduit (Caine et al., 1996). Faults with a large offset may contain a high percentage of clay and act as barriers for fluid flow in reservoirs (Benson and Person, 2006). This barrier effect leads to pressure build-up and subsequent stress changes that may reduce fault stability and eventually induce felt seismicity (Vilarrasa et al., 2016). Even for a small fault offset, permeability across the fault in reservoir sections may decrease as a result of mineral precipitation after hydrothermal water circulation. As for fault permeability in the caprock sections, shear failure may induce an increase in permeability with respect to that of the intact rock, though the creation of conduits for CO_2 upward migration is unlikely due to caprock ductility (Laurich et al., 2014; Bourg, 2015).

Opalinus clay (a Jurassic shale from Switzerland) is considered to be a representative caprock material because of its high (~60%) clay content and very small dominant pore size (~30 nm). Injection of CO_2 inside low-permeable clayey specimens, their relative permeability to brine and CO_2, and CO_2 breakthrough pressure are discussed in Makhnenko et al. (2017). Poromechanical properties of the shale are analysed by performing drained, undrained, and unjacketed conventional triaxial tests (Räss et al., 2017). Thermo-hydro-mechanical response of the caprock due to cooling is discussed in Vilarrasa et al. (2015a), who showed that a potential shallow (~1 km) storage case with cold CO_2 injection leading to caprock cooling by 20 ˚C (from 40 ˚C to 20 ˚C) does not compromise shale's integrity. Additionally, shales show interesting self-sealing features and their ductile-type failure often allows to retain very small permeability. Viscous (time-dependent) deformation may become significant when assessing the long-term caprock integrity. Creep of Opalinus clay was found to accelerate with temperature and pore fluid pressure raise, which increases the probability of porosity wave creation (Räss et al., 2017).

The overarching goal of this study is to identify the main challenges for caprock integrity (e.g., temperature and chemical effects, long-term permeability, and strength evolution) and to study them both experimentally and numerically for a caprock representative. In addition to our previous laboratory studies on intact shale, we have carried out new experiments on remolded (reconstituted) Opalinus clay that is more permeable and represents a fault material. Once the properties of the rock are determined from laboratory experiments, we model CO_2 injection into an extensive aquifer crossed by a low-permeable fault to assess caprock integrity and discuss the implications for deep geologic storage.

2. EXPERIMENTAL TECHNIQUES

Experimental techniques have been developed to characterize shale behavior. Intact and remolded Opalinus clay specimens are brought to the conditions of deep (> 1 km depth) geologic storage and fully saturated with in-situ brine. The back pressure saturation method is implemented with graduate increase of upstream and downstream pressures, p, and promoting the flow through low-permeable (~ 10^{-20} m^2) specimens. It allows achieving full saturation (at p > 7 MPa) that is confirmed by measurements of constant Skempton's B coefficient values while the effective mean stress is preserved to be the same. Recorded undrained pore pressure increments are corrected for the influence of "dead" volume (Makhnenko and Labuz, 2016).

One of the critical parameters for the barrier sealing efficiency is the breakthrough pressure, i.e., the excess of non-wetting fluid (e.g., CO_2) pressure above initial pore fluid pressure that is enough to initiate its flow through the sealing layer. Tests on thin (12 mm in height and 35 mm in diameter) shale specimens loaded under oedometric conditions allowed evaluating the breakthrough pressure and permeability for liquid (24 ºC) and supercritical CO_2 (42 ºC). Use of thin specimens significantly facilitates saturation and flow tests in low-permeable materials, because the timescale for pore pressure diffusion is proportional to the characteristic specimen length squared. The breakthrough pressure for liquid and supercritical CO_2 is measured using two different methods: direct (with the establishment of continuous CO_2 flow) and indirect (through a residual capillary pressure evaluation). Brine and CO_2 permeability of shale is reported from steady-state flow tests performed at fixed differential pressure for at least three days (Makhnenko et al., 2017).

Poroelastic parameters are measured in drained and undrained conventional triaxial compression experiments with specimens of 50 mm in diameter and 100 mm in height (Makhnenko and Labuz, 2016; Räss et al., 2017). Drained and undrained heating and cooling tests provide the corresponding thermal expansion coefficients. Upon completion of elastic parameters' measurements, intact and remolded shale specimens are loaded to failure. Undrained tests at different effective confining pressures provide failure data to evaluate cohesion and friction of tested rocks. Considering the characteristic timescale to guarantee pore pressure equilibration in triaxial tests, the overall duration of each test that included back pressure saturation process, measurements of elastic properties, and loading to failure is 4-6 weeks.

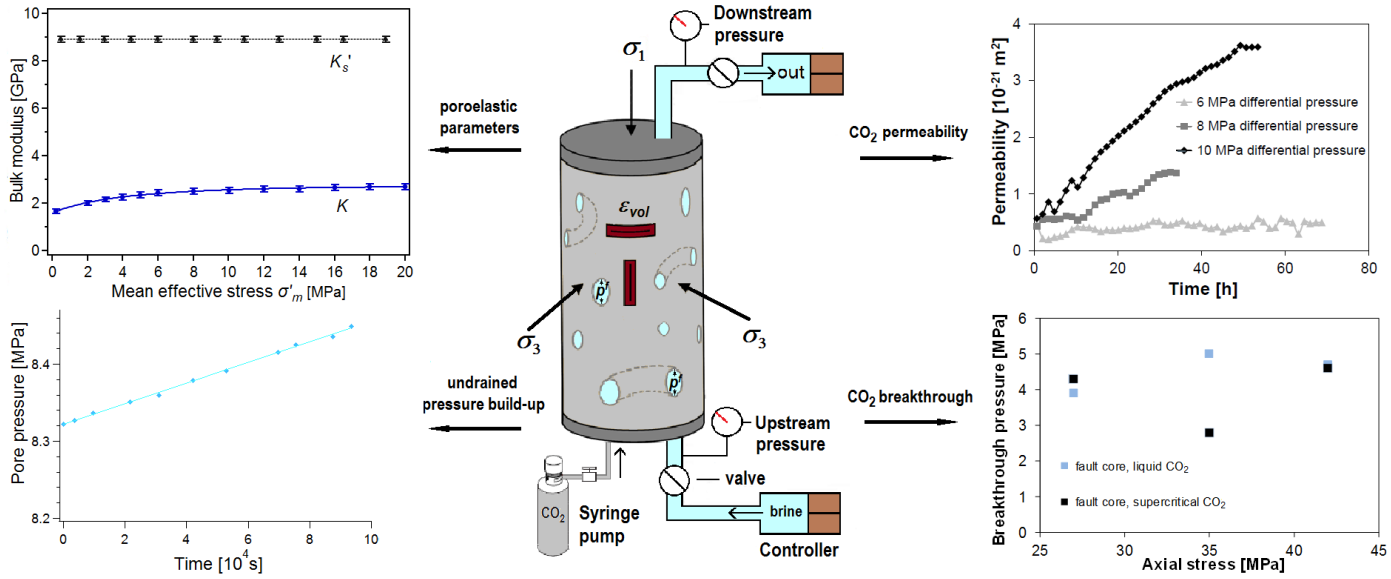

Fig. 2. Overview of the tests performed on clay-rich materials.

3. MODEL FORMULATION

We model CO_2 injection in a deep saline aquifer that is crossed by a low-permeable fault (Figure 3). The fault dips 60º and is formed by a fault core and a damage zone on both sides of the core. While the fault core has the same properties along the whole fault, the damage zone has different properties for each rock type. We assume that CO_2 is injected through a horizontal injection well that is parallel to the fault, so we model a 2D plane strain cross section.

The injection well, which is placed 5 m above the bottom of the injection formation, is located 1 km away from the fault. The model extents laterally for 15 km to each side of the fault. The storage formation, which represents Berea sandstone, overlays (base rock) and is overlain (caprock) by Opalinus clay, which properties vary slightly as a function of depth. Below the base rock, we model the upper 100 m of the crystalline basement, which is made of Charcoal granite. Above the caprock, another saline aquifer, made of Indiana limestone, is included in the model. The top of this upper aquifer is placed at a depth of 1,275 m. The geological layers above this aquifer are not included in the model, but its equivalent weight is applied as an overburden at the top of the model.

We consider a normal faulting stress regime that is coherent with the presence of the steep fault. The vertical stress is given by the weight of the rock, which is considered to have an average of 23 MPa/km. The horizontal stresses are $\sigma_H = \sigma_h = 0.69\sigma_v$. The mechanical boundary conditions are given by a constant vertical stress at the top of the model equal to 29.3 MPa and no displacement perpendicular to the lateral and bottom boundaries. We consider a temperature of 60 ºC, which corresponds to a surface temperature of 10 ºC and the geothermal gradient of 33 ºC/km at 1.5 km, i.e., the depth of the storage formation. Water pressure is assumed to be hydrostatic and constant pressure boundary conditions are applied at the lateral boundaries. At the well, CO_2 is injected at a rate of $2.0\cdot10^{-3}$ kg/s/m for 1 year.

We solve this hydro-mechanical problem in a fully coupled way. The hydraulic problem is governed by mass and momentum conservation of each phase, i.e., water and CO_2. Mass conservation of each fluid is given by

$$\frac{\partial(\varphi S_\alpha \rho_\alpha)}{\partial t} + \nabla\cdot(\rho_\alpha \mathbf{q}_\alpha) = r_\alpha, \qquad \alpha = c, w \qquad (1)$$

where φ is porosity, S_α is saturation of α-phase, ρ_α is density of α-phase, t is time, $\mathbf{q}_\alpha$ is the volumetric flux of α-phase, which is given by momentum conservation, r_α is the phase change term, and α is either CO_2-rich phase, c, or aqueous phase, w. The momentum conservation for slow laminar flow in permeable porous media is described by Darcy's law (Bear, 1972).

The mechanical problem is governed by the momentum balance of the solid phase. If inertial terms are neglected, the momentum balance reduces to the equilibrium of stresses

$$\nabla\cdot\boldsymbol{\sigma} + \mathbf{b} = \mathbf{0} \qquad (2)$$

where $\boldsymbol{\sigma}$ is the stress tensor and $\mathbf{b}$ is the body forces vector.

We assume that rocks behave elastically, so the stress-strain relationship is given by Hooke's law

$$\boldsymbol{\varepsilon} = \frac{\sigma'_m}{3K}\mathbf{I} + \frac{1}{2G}\left(\boldsymbol{\sigma}' - \sigma'_m\mathbf{I}\right) \qquad (3)$$

where $\boldsymbol{\varepsilon}$ is the elastic strain tensor, $\sigma'_m = \mathrm{tr}(\boldsymbol{\sigma}')/3$ is the mean effective stress, $K = E/3(1-2\nu)$ is the bulk modulus,

$G = E/(2(1+\nu))$ is the shear modulus, E is Young's modulus, ν is Poisson's ratio, $\mathbf{I}$ is the identity matrix, and $\boldsymbol{\sigma}' = \boldsymbol{\sigma}' - p\mathbf{I}$ is the effective stress tensor. We adopt compression positive sign convention.

We numerically simulate this problem using CODE_BRIGHT (Olivella et al., 1996), which is a fully coupled finite element code capable of solving non-isothermal two-phase flow in deformable porous media. The model has been discretized using a mesh of 5775 quadrilateral elements, having a higher refinement around the fault and the injection well.

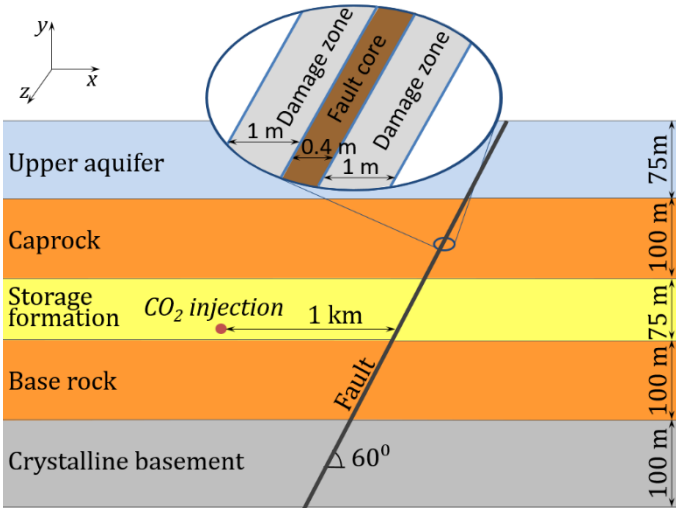

Figure 3. Geometry of the model with CO_2 injection through a horizontal well parallel to a low-permeable fault.

4. RESULTS

Remolded and intact Opalinus clay specimens are fully saturated with in-situ brine at 8 MPa after two weeks of gradual back pressure increase. Permeability and poroelastic properties are studied for the mean stress values ranging from 10 to 28 MPa. Intrinsic permeability for remolded shale is ~ 10^{-20} m^2, while intrinsic permeability of the intact material is ~ 10^{-21} m^2. Mercury intrusion porosimetry (MIP) measurements performed on the tested samples show a mono-modal pore size distribution with a peak at 21 nm inter-platelet distance for remolded shale and 15 nm for the intact material. Pores of this size are supposed to be flat (crack-like) and localized in the clay matrix. Porosity of intact specimens is 0.12 and remolded shale specimen porosity is evaluated to be 0.15 at the range of applied stresses (Cassini et al., 2017).

Breakthrough pressure is found to be slightly increasing with effective stress, but is independent of temperature and CO_2 phase. For the range of stresses considered in the model, the breakthrough pressure is measured to be 9-10 MPa for intact shale and 3-5 MPa for the remolded material. CO_2 effective permeability (i.e., intrinsic permeability times CO_2 relative permeability) of brine-saturated shale is at least an order of magnitude smaller than the one for brine and is ~ 10^{-22} m^2 for the intact and reconstituted material loaded to in-situ conditions (Makhnenko et al., 2017).

The characteristic time for pore pressure equilibration in triaxial specimens is on the order of tens of hours, and each pressure step in our experiments requires three days to reach consistent measurements. Drained and undrained Young's modulus in shale is increasing with mean effective stress and for the simulated in-situ conditions is taken as 2.3 and 4.0 GPa, respectively. Undrained Poisson ratio is 0.40 and 0.42 for intact and remolded shale, respectively. Cohesion and friction angles for intact and remolded shale are determined from undrained triaxial compression data, and provide the same friction angle for both materials, being equal to 24º. However, it may change with the applied mean stress. Cohesion is measured to be 6 MPa for intact shale and below 1 MPa for the remolded material.

Elastic properties, friction, and cohesion for reservoir, upper aquifer and crystalline basement are obtained from triaxial tests performed on these rocks (Labuz and Biolzi, 1998; Makhnenko and Labuz, 2014; Makhnenko et al., 2015). Gas entry pressure and porosity values are obtained from MIP tests. CO_2 will flow relatively easy in the storage formation due to its high permeability and low entry pressure. On the other hand, the low permeability and high entry pressure of shale (Makhnenko et al., 2017) will confine CO_2 in the storage formation and prevent CO_2 leakage through the caprock.

Values of porosity for the confining layers, crystalline basement, and the fault core are taken as the effective porosities, i.e., those that contribute to flow. Relative CO_2 and water permeabilities are taken as power functions of saturation, with a power of three for the sandstone and the limestone and six for the shale and the granite (Bennion and Bachu, 2008). Low-permeability (~ 10^{-21} m^2) and relatively low (~ GPa) elastic moduli of caprock and baserock provide characteristic diffusion time for these formations to be ~ 10^9 sec (tens of years), and hence the undrained elastic properties of shale were considered.

Fault core is made of remolded shale, which properties along with the properties of other damaged materials may vary depending on level of damage and applied effective stress. The friction angle of siliciclastic and carbonate rocks (aquifers), is high, above 30º, but it is low (< 30 º) for clay-rich materials, such as caprock and fault core (Vilarrasa et al., 2016). Thus, the aquifers are likely to be far from being critically stressed, but the clay-rich materials may be close to shear failure conditions. With the assumptions of purely drained (for the storage formation, upper aquifer, basement, fault core, and damage zones) or undrained (caprock and baserock) behavior, linear failure properties independent of intermediate principal stress, and power law type dependence of water and CO_2 permeabilities from the

degree of saturation, the introduced model is assumed to be a first order approach to the problem of CO_2 injection in semi-closed aquifers.

We use the material properties determined in the laboratory as input data in our numerical model. Simulation results allow us to assess caprock integrity when injecting CO_2 in the vicinity of low-permeable faults. The injected CO_2 forms a CO_2-rich phase that advances upwards due to buoyancy (Figure 4). Furthermore, the CO_2 plume is displaced away from the low-permeable fault because of the higher pressure build-up induced between the fault and the injection well. CO_2 injected at the bottom of the storage formation reaches the bottom of the caprock after 11 months. The low permeability and high entry pressure of the caprock hinders upward CO_2 migration across it. Thus, CO_2 advances laterally through the top of the storage formation. Nevertheless, caprock sealing capacity might be compromised if overpressure induces failure conditions in it.

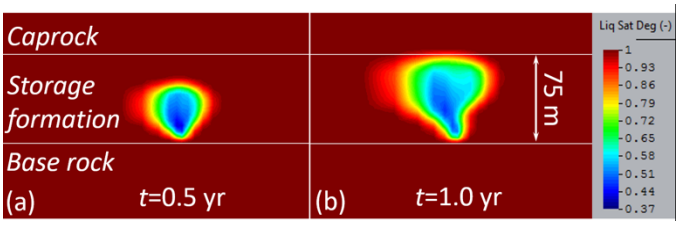

Figure 4. CO_2 plume after (a) 0.5 years and (b) 1 year of injection. The low-permeable fault is located on the right-hand side of the injection well and, thus CO_2 tends to advance towards the left-hand side.

To assess caprock integrity, both fluid pressure and stress evolution should be analysed. Figure 5 displays fluid pressure evolution above the injection well at the top of the storage formation and in the caprock 5 m above the storage formation.

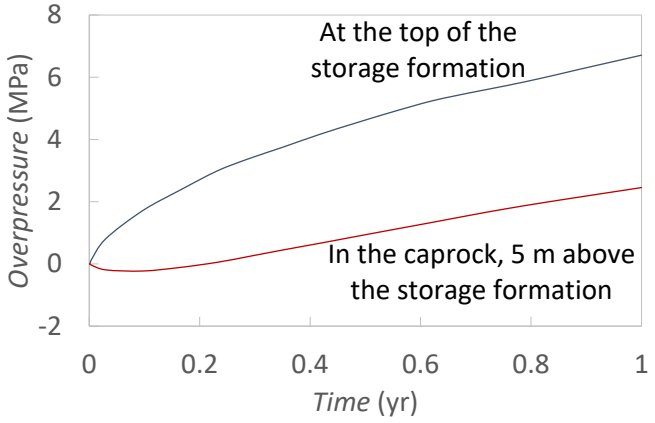

Figure 5. Overpressure evolution above the injection well at the top of the storage formation and in the caprock, 5 m above the storage formation-caprock interface.

While fluid pressure continuously increases in the storage formation, it initially drops in the lower portion of the caprock due to coupled hydro-mechanical effect (Hsieh, 1996). This behavior is referred as Noordbergum effect and is caused by an expansion of the caprock pore volume induced by the bending of the caprock that occurs in response to the initial expansion of the storage formation as it is pressurized (Vilarrasa et al., 2013).

Figure 6 shows the Mohr circles at a point in the caprock placed 5 m above the storage formation and right above the injection well. Initially, the stress state is close to the yield surface. At the early stages of injection (first two months), fluid pressure drops in the caprock (Figure 5), which improves caprock stability (see the blue circle). However, as the injection continues, pressure starts increasing, bringing the stress state closer to the yield surface. After one year of injection, the stress state approaches the yield surface. Note that, apart from being displaced to the left, the Mohr circle decreases in size. This shrinkage occurs because horizontal total stresses increase as a result of lateral confinement that opposes pressure build-up.

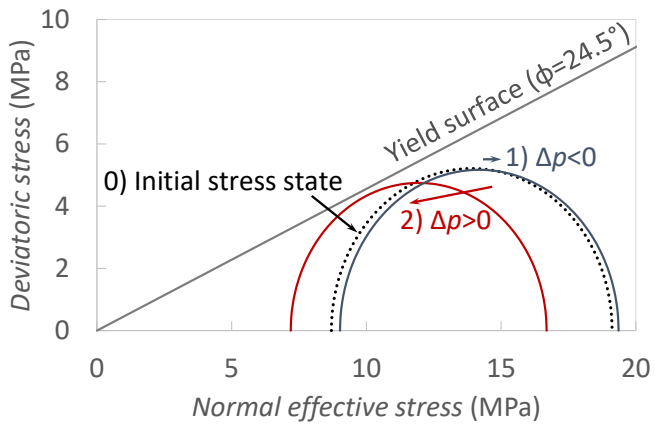

Figure 6. Mohr circles plotted at a point of the caprock placed above the injection well and 5 m above the storage formation. The black dotted circle is the initial stress state, the blue circle is the state one month after the injection starts, coinciding with the minimum fluid pressure at the caprock, and the red circle is the resulting stress state after one year of injection.

Figure 7 displays the liquid pressure distribution around the fault after one year of injection. The low-permeable fault core effectively acts as a barrier to flow, causing a high pressurization of the compartment of the storage formation where CO_2 is injected, but preventing overpressure to propagate across the fault. Despite this additional pressurization caused by the low-permeable fault, the caprock does not yield for the simulated CO_2 injection in the vicinity of the injection well because of the horizontal total stress increase (Figure 6).

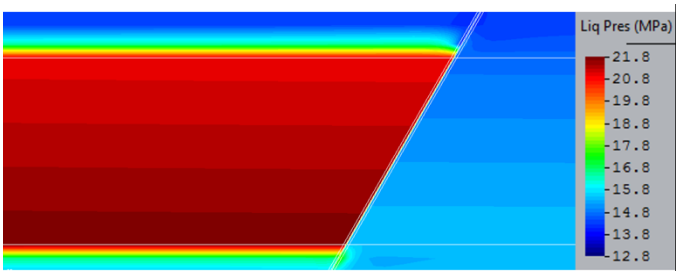

Figure 7. Liquid pressure distribution around the low-permeable fault after one year of injection. While the hanging wall, where the injection well is located, is highly pressurized, the footwall maintains the initial liquid pressure.

5. DISCUSSION

Clay-rich geomaterials have low frictional strength, which may lead to microseismicity induced by CO_2 injection (Figure 6). However, the ductility of clay-rich geomaterials is likely to maintain the permeability low, so no CO_2 leakage across caprock will occur. Our tests with the shale and remolded shale specimens show that brine permeability of failed specimens increases by a factor smaller than 2, which is not compromising the sealing capacity of low-permeable rock. Furthermore, we assume that the horizontal stress gradients are constant with depth. However, the stress state tends to be more isotropic, i.e., lower (than the assumed) deviatoric stress in soft geological layers, like shales (Hergert et al., 2015). A lower deviatoric stress would imply a smaller Mohr circle that is placed further away from the yield surface. Therefore, caprocks are not likely to yield despite of their low frictional strength.

Another concern related to caprock integrity is cooling of the caprock. In the considered setting where CO_2 is injected at the bottom of a thick storage formation, the cooling front will take a long time, in the order of the decades, to reach the bottom of the caprock (Vilarrasa et al., 2015b). However, if the caprock was cooled down, a thermal stress reduction would be induced, bringing the stress state closer to shear failure conditions. On the other hand, cooling will reduce the pore pressure and increase effective confinement because the thermal expansion coefficient of brine is higher than that of the rock (Vilarrasa et al., 2015a). Thus, to minimize the risk of damaging the caprock, the location of injection wells should be analyzed in each storage site.

The presence of low-permeable faults crossing the storage formation will lead to an additional pressurization of a part of the storage formation. This overpressure taking place just on one side of a fault may lead to stress changes that could destabilize the fault (Gheibi et al., 2016). This instability may cause felt induced seismicity if the fault is brittle (Cappa and Rutqvist, 2011) or microseismicity or even aseismic slip if the fault is ductile (Cornet et al., 1997). In sedimentary basins with multiple caprock and reservoir layers, faults are likely to be constituted by a significant proportion of clay, making them ductile (Egholm et al., 2008). Hence, if the fault was reactivated, its ductility would give rise to rather low seismic events.

6. CONCLUSION

Experimentally measured parameters are used to simulate shaly caprock and fault deformation and stability for the case of geologic carbon dioxide storage, where cooling is likely to occur around injection wells. Simulation results show that the caprock is unlikely to yield, even for low frictional strength, because the horizontal total stresses increase in response to an overpressure, reducing the deviatoric stress. Additionally, it is found that clay-rich faults may induce microseismic events, but without leading to CO_2 leakage, due to the ductility of clay-rich geomaterials.

ACKNOWLEDGMENTS

R. Makhnenko acknowledges partial support from the Center for Geologic Storage of CO_2, an EFRC funded by the U.S. DOE, Office of Science, BES, under Award DE-SC0C12504. V. Vilarrasa acknowledges financial support from the “TRUST" project (European Community's Seventh Framework Programme FP7/2007-2013 under grant agreement n 309607) and from “FracRisk" project (European Community's Horizon 2020 Framework Programme H2020-EU.3.3.2.3 under grant agreement n 640979).

REFERENCES

1. Bear, J. (ed.) 1972. *Dynamics of fluids in porous media*. New York: Elsevier.
2. Bennion, B. and S. Bachu. 2008. Drainage and imbibition relative permeability relationships for supercritical CO_2/brine and H_2S/brine systems in intergranular sandstone, carbonate, shale, and anhydrite rocks. *SPE Reservoir Evaluation & Engineering* 11(03): 487-496.
3. Bense, V.F. and M.A. Person. 2006. Faults as conduit-barrier systems to fluid flow in siliciclastic sedimentary aquifers. *Water Resour. Res.* 42(5): W05421.
4. Bourg, I.C. 2015. Sealing shales versus brittle shales: a sharp threshold in the material properties and energy technology uses of fine-grained sedimentary rocks. *Environ. Sci. Tech. Lett.* 2: 255-259.
5. Caine, J.S., J.P. Evans, and C.B. Forster. 1996. Fault zone architecture and permeability structure. *Geology* 24(11): 1025-1028.
6. Cappa, F. and J. Rutqvist. 2011. Impact of CO_2 geological sequestration on the nucleation of earthquakes. *Geophys. Res. Letters* 38(17): L17313.

7. Cassini, E., D. Mylnikov, and R. Makhnenko. 2017. Chemical influence of pore pressure on brine flow in clay-rich material. In: A. Ferrari and L. Laloui (eds), *Advances in Laboratory Testing and Modelling of Soils and Shales (ATMSS)*, Springer Series in Geomechanics and Geoengineering, 273-280.

8. Cornet, F.H., J. Helm, H. Poitrenaud, and A. Etchecopar. 1997. Seismic and aseismic slips induced by large-scale fluid injections. In *Seismicity Associated with Mines, Reservoirs and Fluid Injections*, 563-583. Basel: Birkhäuser.

9. Egholm, D.L., O.R. Clausen, M. Sandiford, M.B. Kristensen, and J.A. Korstgård. 2008. The mechanics of clay smearing along faults. *Geology* 36(10): 787-790.

10. Gheibi, S., R.M. Holt, and V. Vilarrasa. 2016. Stress path evolution during fluid injection into geological formations. In *Proceedings of 50th US Rock Mechanics/Geomechanics Symposium, Houston, TX, 26-29 June 2016*, paper No. 620.

11. Hergert, T., O. Heidbach, K. Reiter, S.B. Giger, and P. Marschall. 2015. Stress field sensitivity analysis in a sedimentary sequence of the Alpine foreland, northern Switzerland. *Solid Earth* 6(2): 533-552.

12. Hesse, M.A., F.M. Orr, and H.A. Tchelepi. 2008. Gravity currents with residual trapping. *J. Fluid Mech.* 611: 35-60.

13. Hsieh, P.A. 1996. Deformation-induced changes in hydraulic head during ground-water withdrawal. *Ground Water* 34(6): 1082-1089.

14. IEAGHG. 2011. Caprock systems for CO_2 geological storage. IEA Environmental Projects Ltd.

15. Labuz, J.F. and L. Biolzi. 1998. Characteristic strength of quasi-brittle materials. *Int. J. Solids Struct.* 35(31-32): 4191-4203.

16. Laurich, B., J.L. Urai, G. Desbois, C. Vollmer, and C. Nussbaum. 2014. Microstructural evolution of an incipient fault zone in Opalinus Clay: Insights from an optical and electron microscopic study of ion-beam polished samples from the Main Fault in the Mt-Terri Underground Research Laboratory. *J. Struct. Geol.* 67: 107-128.

17. Makhnenko, R. and J. Labuz. 2014. Plane strain testing with passive restraint. *Rock Mech. Rock Eng.* 47(6): 2021-2029.

18. Makhnenko, R.Y., J. Harvieux, and J.F. Labuz. 2015. Paul-Mohr-Coulomb failure surface of rock in the brittle regime. *Geophys. Res. Lett.* 42: 6975-6981.

19. Makhnenko, R.Y. and J.F. Labuz. 2016. Elastic and inelastic deformation of fluid-saturated rock. *Phil. Trans. R. Soc. A* 374: 20150422.

20. Makhnenko, R.Y., V. Vilarrasa, D. Mylnikov, and L. Laloui. 2017. Hydromechanical aspects of CO_2 breakthrough into clay-rich caprock. *Energy Procedia* doi: 10.1016/j.egypro.2017.03.1453.

21. Olivella, S., A. Gens, J. Carrera, and E.E. Alonso. 1996. Numerical formulation for a simulator (CODE_BRIGHT) for the coupled analysis of saline media. *Eng. Computations* 13(7): 87-112.

22. Paterson, L., M. Lu, L. Connell, and J.P. Ennis-King. 2008. Numerical modeling of pressure and temperature profiles including phase transitions in carbon dioxide wells. In *Proceedings of SPE Annual Technical Conference and Exhibition, Denver, CO, 21-24 September 2008.*

23. Räss, L., R.Y. Makhnenko, Y. Podladchikov, and L. Laloui. 2017. Quantification of viscous creep influence on storage capacity of caprock. *Energy Procedia* doi: 10.1016/j.egypro.2017.03.1455.

24. Rutqvist, J., A.P. Rinaldi, F. Cappa, P. Jeanne, A. Mazzoldi, L. Urpi, Y. Guglielmi, and V. Vilarrasa. 2016. Fault activation and induced seismicity in geological carbon storage–Lessons learned from recent modeling studies. *J. Rock Mech. Geotech. Engng.* 8(6): 789-804.

25. Song, J. and D. Zhang. 2013. Comprehensive review of caprock-sealing mechanisms for geologic carbon sequestration. *Env. Sci. & Tech.* 47(1): 9-22.

26. Verdon, J.P., J.M. Kendall, D.J. White, and D.A. Angus. 2011. Linking microseismic event observations with geomechanical models to minimise the risks of storing CO_2 in geological formations. *Earth Planet. Sci. Lett.* 305(1): 143-152.

27. Vilarrasa, V., D. Bolster, S. Olivella, and J. Carrera. 2010. Coupled hydromechanical modeling of CO_2 sequestration in deep saline aquifers. *Int. J. Greenhouse Gas Control* 4(6): 910-919.

28. Vilarrasa, V., J. Carrera, and S. Olivella. 2013. Hydromechanical characterization of CO_2 injection sites. *Int. J. Greenhouse Gas Control* 19: 665-677.

29. Vilarrasa, V., R. Makhnenko, and L. Laloui. 2015a. Influence of poromechanical and thermal properties of the caprock on the safety of CO_2 storage. In *Proceedings of Second EAGE Workshop on Geomechanics and Energy, Celle, Germany 13-15 October 2015.*

30. Vilarrasa, V., J. Rutqvist, and A.P. Rinaldi. 2015b. Thermal and capillary effects on the caprock mechanical stability at In Salah, Algeria. *Greenh. Gases: Sci. & Tech.* 5(4): 449-461.

31. Vilarrasa, V., R. Makhnenko, and S. Gheibi. 2016. Geomechanical analysis of the influence of CO_2 injection location on fault stability. *J. Rock Mech. Geotech. Engng.* 8(6): 805-818.

32. Vilarrasa, V. and J. Rutqvist. 2017. Thermal effects on geologic carbon storage. *Earth-Sci. Rev.* 165: 245-256.